Class E/F$_3$ Tuned Power Oscillator

Tsuyoshi Inaba, *Student Member, IEEE*, and Hirotaka Koizumi, *Member, IEEE*

***Abstract*—This paper proposes a Class E/F$_3$ tuned power oscillator based on the Class E/F$_3$ amplifier. The oscillator has a feedback-loop circuit and starts the oscillation in automatic. In addition, the oscillator achieves zero-voltage switching and zero-voltage derivative switching; therefore, the switching losses are reduced under high oscillation frequency. Moreover, the third harmonic tuned by providing a third harmonic series resonant circuit reduces the switch voltage stress of the MOSFET sufficiently. The oscillator was designed, built and tested using an IRFR120Z power MOSFET. Under the condition of the input voltage 6.003 V, following results were shown: the measured oscillation frequency was 801.6 kHz, the output power was 0.9075 W, and the power conversion efficiency was 86.24%.**

***Index Terms*—Class E/F$_3$, high frequency, tuned power oscillator.**

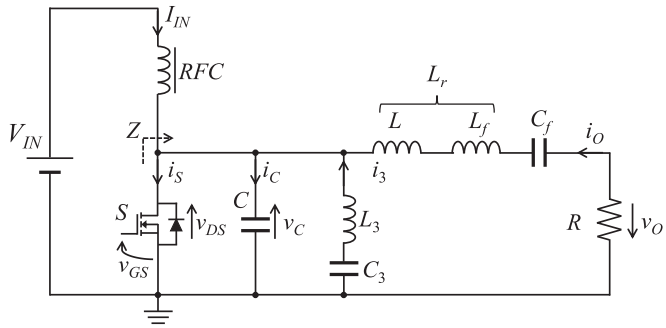

Fig. 1. Circuit topology of the Class E/F$_3$ amplifier [20].

I. Introduction

RECENTLY, due to the advancement of wireless communication systems, communication devices need to show high-performance, be miniaturized, and have low cost. To downsize these devices, miniaturizing the passive elements of the RF power amplifiers is required. To meet such demand, these amplifiers need to be operated at high frequency with high efficiency [1], [2]. However, switching losses of the switching devices increase at high frequency.

Class E amplifier [3]–[6] is one of the classes of the RF tuned power amplifiers [7], [8] and maintains high efficiency even if it is used at high frequency, which is achieved by zero-voltage switching (ZVS) and zero-voltage derivative switching (ZVDS) at the turning ON. However, the switch voltage stress becomes high for the Class E power amplifier.

Class F amplifiers [1], [11], [12] have multiple resonant filters of the odd harmonics to control the finite number of the harmonic components of the switch voltage and current waveforms. In the case of Class F power amplifier, the resonant filters of the odd harmonics make the switch voltage square waveform and the switch current half-sinusoidal waveform. On the other hand, in the case of Class F^{-1}, the resonant filters of the even harmonics make the switch voltage half-sinusoidal waveform and the switch current square waveform.

Applying the same technique of the Class F power amplifier or the Class F^{-1} power amplifier to the Class E amplifier, the switch voltage or current stress can be reduced. Class E/F$_3$ power amplifier [16]–[20], which is one of such amplifiers, has a series resonant circuit tuned to the third harmonic component, which reduces the switch voltage stress.

Class E oscillator [21]–[25] is expected in various places, most notably in fluorescent lamp, dc/ac inverter, dc/dc converter, plasma driver, laser driver, and so on. When a positive feedback-loop circuit is applied to the Class E amplifier, the amplifier operates as the Class E oscillator. The oscillator starts running oscillation automatically when the input voltage is impressed, and it achieves ZVS and ZVDS at the turning ON instant. The Class E oscillator also has a disadvantage of the high switch voltage stress.

In this paper, Class E/F$_3$ tuned power oscillator is proposed. The oscillator is based on the Class E/F$_3$ amplifier, which achieves ZVS and ZVDS at the turning-on instant. The Class E/F$_3$ oscillator is expected to be used for applications similar to the Class E oscillator, and low voltage stress is realized. Owing to a series resonant circuit tuned to the third harmonic, the switch voltage stress is reduced by about 22% compared to the Class E oscillator. Therefore, the range of device selection is broadened and a device with a small on-resistance can be selected.

In Section II, the circuit topology and the design equations of the Class E/F$_3$ tuned power amplifier are reviewed. In Section III, the circuit topology and an analysis of the Class E/F$_3$ tuned power oscillator are shown. In Sections IV and V, the simulation result and the experimental results are shown.

II. Class E/F$_3$ Tuned Power Amplifier

Fig. 1 shows a circuit topology of the Class E/F$_3$ tuned power amplifier [20], which consists of an input voltage $V_{\rm IN}$, a radio frequency choke RFC, a shunt capacitor C, a series resonant circuit L_3–C_3, a resonant inductor L_r, a resonant capacitor C_f, and a load resistance R. The inductor L_r can be regarded as a

Manuscript received February 9, 2016; accepted March 8, 2017. Date of publication March 23, 2017; date of current version November 2, 2017. Recommended for publication by Associate Editor M. A. E. Andersen. *(Corresponding author: Tsuyoshi Inaba.)*

The authors are with Tokyo University of Science, Tokyo 125-8585, Japan (e-mail: T.I.1993@ieee.org; littlespring@ieee.org).

Color versions of one or more of the figures in this paper are available online at http://ieeexplore.ieee.org.

Digital Object Identifier 10.1109/TPEL.2017.2686900

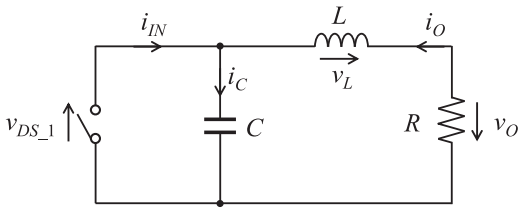

Fig. 2. Equivalent load network of the Class E/F$_3$ amplifier at fundamental frequency.

series connection of an inductor L and an inductor L_f, which is a part of the series resonant circuit C_f–L_f tuned to the operation frequency f. Further, a series resonant circuit L_3–C_3 is tuned to the third harmonic components $3f$. Therefore, the impedance of the series resonant circuit L_3–C_3 is zero for the third harmonic, and it is infinite for the other harmonics.

The optimum switch voltage waveform of the Class E/F$_3$ amplifier fulfills Class E conditions. It is obtained by appropriate design of the amplifier. Assuming the duty cycle $D = 0.5$, we can use the waveform formulas from [20]. The switch current i_S for $0 < \omega t \le 2\pi$ is

$$i_S(\omega t) = \begin{cases} I_{\rm IN} + I_O \sin(\omega t + \varphi) + I_3 \sin 3\omega t, & [0 < \omega t \le \pi] \\ 0, & [\pi < \omega t \le 2\pi] \end{cases} \tag{1}$$

where $I_{\rm IN}$ is the dc input current, I_O is the amplitude of the output current, φ is the initial phase angle of the output current, and I_3 is the amplitude of the current through the series resonant circuit L_3–C_3. The switch voltage $v_{\rm DS}$ are shown in (2)

$$v_{\rm DS}(\omega t) = \begin{cases} 0 & [0 < \omega t \le \pi] \\ \dfrac{I_{\rm IN}}{\omega C}\left\{\omega t - \pi - \dfrac{I_3}{3}(1 + \cos 3\omega t)\right. & \\ \qquad \left. - I_O\left[\cos(\omega t + \varphi) + \cos\varphi\right]\right\} & [\pi < \omega t \le 2\pi]. \end{cases} \tag{2}$$

Parameters for design are given as the initial phase angle of the output current $\varphi = \arctan\{18\pi/(8 - 9\pi^2)\} = -0.6105\,[\text{rad}] = -34.98\,[\text{deg}]$, the road resistance $R = 0.6576 V_{\rm IN}^2/P_O$, the normalized reactance of ωL with R $\omega L/R = 0.9599$, and the normalized resistance R with the reactance of $1/\omega C$ $\omega CR = 0.2094$ in [20, Eqs. (21)–(23)].

Fig. 2 shows an equivalent load network of the Class E/F$_3$ amplifier at the fundamental frequency. The current through the inductor L is sinusoidal waveform because the load quality factor Q of the series resonant circuit C_f–L_f is enough high. Impedance of the series resonant circuit C_f–L_f can be regarded as zero for the fundamental frequency and infinite for the other harmonics. Therefore, it is sufficient to decide the input impedance of the load network at only the operation frequency f. From Fig. 2, the fundamental component of the switch voltage

TABLE I
COMPARISON OF THE CLASS E AMPLIFIER AND CLASS E/F$_3$ AMPLIFIER IN TERMS OF THE NORMALIZED VOLTAGE/CURRENT STRESS

	Normalized voltage stress $V_{\rm DS}/V_{\rm IN}$	Normalized current stress $I_S/I_{\rm IN}$
Class E amplifier [9] ($D = 0.5$)	3.562	2.862
Class E/F$_3$ amplifier [20] ($D = 0.5$)	3.142	3.056

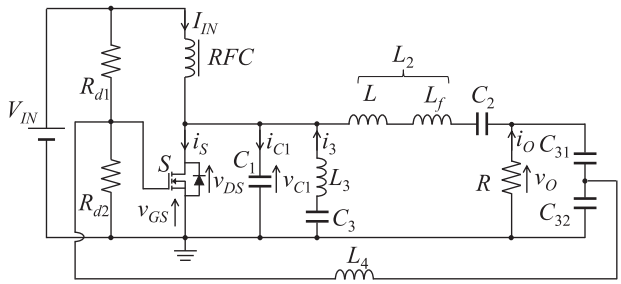

Fig. 3. Circuit topology of the Class E/F$_3$ tuned power oscillator.

at the operation frequency $v_{\rm DS\_1}$ is

$$\begin{aligned} v_{\rm DS\_1} &= -v_O - v_L = -[V_O \sin(\omega t + \varphi) + \cos(\omega t + \varphi)] \\ &= -V_{\rm DS\_1} \sin(\omega t + \varphi + \psi) \end{aligned} \tag{3}$$

where $V_{\rm DS\_1}$ is the amplitude of the fundamental components of the switch voltage, and ψ is the phase angle of the load network at the operation frequency which is $\psi = \arctan(\omega L/R) = \arctan(0.9599) = 43.85\,[\text{deg}]$. Finally, we obtain

$$v_{\rm DS\_1} = V_{\rm DS\_1} \sin(\omega t + 3.297). \tag{4}$$

A comparison of the Class E amplifier and the Class E/F$_3$ amplifier in terms of the normalized voltage/current stress is shown in Table I.

III. CLASS E/F$_3$ TUNED POWER OSCILLATOR

Fig. 3 shows a circuit topology of the Class E/F$_3$ tuned power oscillator. The oscillator consists of an input voltage $V_{\rm IN}$, two dividing resistors R_{d1} and R_{d2}, a radio frequency choke RFC, a switch S, a shunt capacitor C_1, a series resonant circuit L_3–C_3 tuned to the third harmonic of the fundamental frequency, an inductor L_2, a capacitor C_2, a load resistance R, and a feedback-loop circuit composed of capacitors C_{31}, C_{32}, and an inductor L_4. Here, the inductor L_2 can be regarded as a series connection of an inductor L and an inductor L_f, which is a part of the series resonant circuit C_2–L_f tuned to the operation frequency f. The switch on duty cycle D is fixed at 0.5 and the gate signal is sinusoidal.

The ideal waveforms for the proposed oscillator are shown in Fig. 4, where $I_{\rm IN}$ is the input current, i_C is the current through the shunt capacitor C_1, i_3 is the current through the series resonant circuit L_3–C_3, i_S is the current through switch S, $v_{\rm DS}$, and v_{C1} are the drain–source voltage of the switch S, i_O is the output

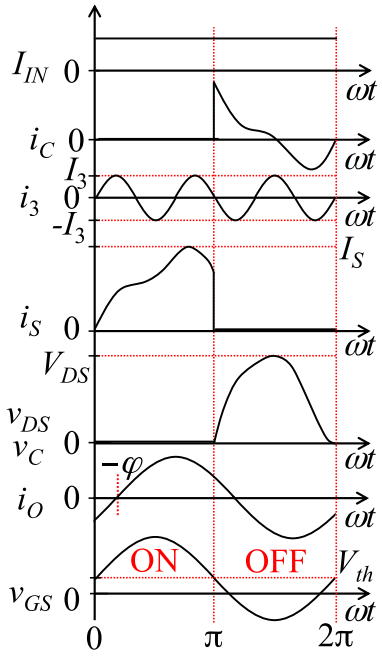

Fig. 4. Ideal waveforms for class E/F$_3$ tuned power oscillator.

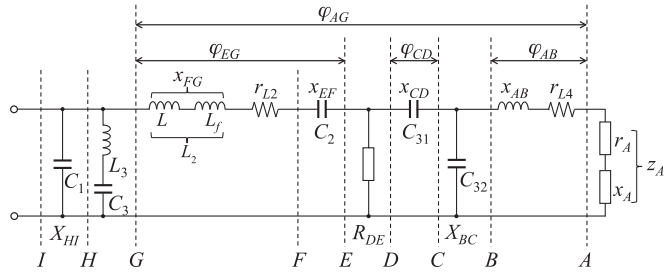

Fig. 5. Equivalent circuit of the Class E/F$_3$ oscillator.

current, and v_{GS} is the gate–source voltage. V_{th} is the threshold voltage of the switch.

A. Optimum Operation Condition of the Class E/F$_3$ Tuned Power Oscillator

The design method of the Class E oscillator is given in [21]–[25]. The Class E/F$_3$ tuned power oscillator can be designed with the same method as that of the Class E oscillator.

An equivalent circuit of the Class E/F$_3$ tuned power oscillator is shown in Fig. 5, which is composed of the load network, the feedback-loop, and the gate–source impedance of the switch. The equivalent circuit is divided into A to I sections for convenience. We give the following assumptions for designing a Class E/F$_3$ tuned power oscillator:

1) the switch S turns ON and OFF instantaneously. Switch S has infinite off-resistance $r_{\rm OFF}$ and no on-resistance $r_{\rm ON}$;
2) the inductors L_2 and L_4 have equivalent series resistance (ESR), and the other passive elements have no ESR;
3) the series resonant circuit L_3–C_3 has zero impedance at the third harmonic and infinite impedance at the other harmonics;

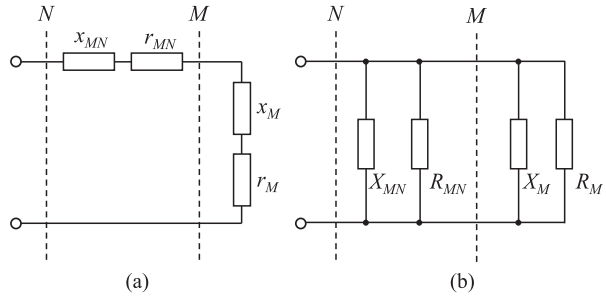

Fig. 6. Notation of the equivalent impedance, (a) a series equivalent impedance, and (b) a parallel equivalent impedance.

4) the loaded quality factor Q of the series resonant circuit L_2-C_2 tuned to the operation frequency f is high enough to make the output current in sinusoidal waveform;
5) the shunt capacitance C_1 includes parasitic drain–source capacitance of switch S;

Fig. 6 shows a notation of the equivalent impedance, where M and N mean arbitrary sections. Fig. 6(a) shows a series equivalent impedance and Fig. 6(b) shows a parallel equivalent impedance. Impedance z_M and admittance Y_M at the M section are

$$z_M = r_M + jx_M = |z_M|e^{j\varphi_M} \tag{5}$$

$$Y_M = \frac{1}{z_M} = \frac{1}{R_M} - j\frac{1}{X_M} \tag{6}$$

where r_M is the series equivalent resistance, x_M is the series equivalent reactance, $|z_M|$ is the absolute value of the equivalent impedance, φ_M is an impedance argument, R_M is the parallel equivalent resistance, and X_M is the parallel equivalent reactance at the M section. Here, the reactance factor q_M to the right of M section is given as

$$q_M = \frac{x_M}{r_M} = \frac{R_M}{X_M}. \tag{7}$$

From (5)–(7), the parallel equivalent resistance R_M and the series equivalent resistance r_M at the M section satisfy the following relations:

$$R_M = r_M\left(q_M^2 + 1\right) \tag{8}$$

$$r_M = \frac{R_M}{q_M^2 + 1}. \tag{9}$$

From (9), the reactance factor q_M is

$$q_M = \pm\sqrt{\frac{R_M}{r_M} - 1}. \tag{10}$$

A relationship between impedance arguments φ_M and φ_N is shown in Fig. 7. The difference φ_{MN} is given by

$$\varphi_{MN} = \varphi_M - \varphi_N = \arctan q_M - \arctan q_N. \tag{11}$$

Equivalent circuits of the feedback-loop and the load network in the stepwise aggregates are shown in Fig. 8.

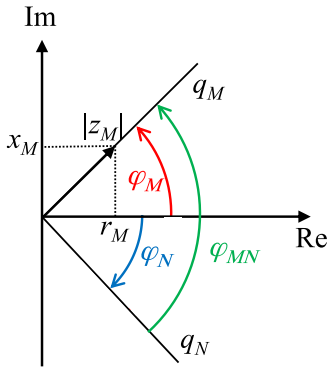

Fig. 7. Relationship between impedance arguments φ_M and φ_N.

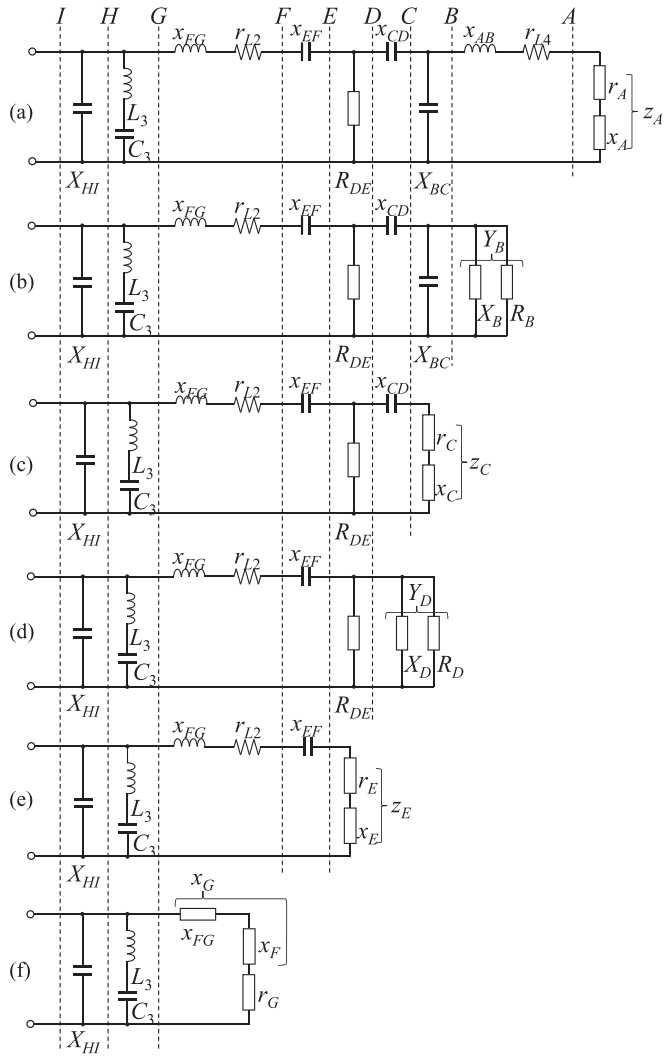

Fig. 8. Equivalent circuits of the feedback-loop and the load network in the stepwise aggregates.

B. Design of the Class E/F$_3$ Tuned Power Oscillator

Initial condition of the Class E/F$_3$ oscillator is given as follows:

1) the output power is $P_O = 1.000$ [W];
2) the input voltage is $V_{\rm IN} = 6.000$ [V];
3) the oscillation frequency is $f = 800.0$ [kHz];
4) the load resistance is $R = 50.00$ [Ω];
5) the ESR r_{L4} of the inductor L_4 is assumed to be 1.000 [Ω];
6) the load quality factor Q is determined as $Q = \omega L_2/R = 12$.

Some part of the output power flows into the feedback-loop circuit. Therefore, the oscillator has to be designed with a value greater than the output power P_O in consideration of the power delivered to the gate resistance of the MOSFET. The extended output power P_O' is

$$P_O' = P_O + P_{\rm loss} + P_g \tag{12}$$

where $P_{\rm loss}$ is the losses consumed in the parasitic components in the oscillator, and P_g is the loss caused in the gate resistance of the MOSFET. Assuming that the power conversion efficiency is $\eta = 90$ [%], the extended output power P_O' is set to

$$P_O' = \frac{P_O}{\eta} = 1.111\,[\rm W]. \tag{13}$$

From the design equation of the Class E/F$_3$ tuned power amplifier and (13), the optimum resistance r_G is

$$r_G = 0.6576\frac{V_{\rm IN}^2}{P_O'} = 21.31\,[\Omega]. \tag{14}$$

From the design equation and (14), the reactance $X_{\rm HI} = -1/(\omega C)$ of the shunt capacitance is

$$X_{\rm HI} = -\frac{1}{0.2094}r_G = -101.8\,[\Omega]. \tag{15}$$

From the design equation and (14), the reactance factor q_G of the G section is given as

$$q_G = \frac{x_G}{r_G} = \frac{\omega L}{r_G} = 0.9599. \tag{16}$$

From (14) and (16), the reactance x_G of the G section is determined as

$$x_G = q_G r_G = 20.46\,[\Omega]. \tag{17}$$

Substituting $Q = 12$ and $r_G = 21.31$ [Ω] into $Q = \omega L_2/R$, we obtain

$$L_2 = \frac{Qr_G}{\omega} = 50.87\,[\mu\rm H] \tag{18}$$

and the reactance x_{FG} in the F–G section is

$$x_{\rm FG} = Q \cdot r_G = 255.7\,[\Omega]. \tag{19}$$

The ESR $r_{L2} = 0.6977$ [Ω] of the L_2 was measured by the impedance meter (HIOKI 3531 Z HiTESTER). Because no resistive component exists except r_{L2}, r_E is obtained as

$$r_E = r_G - r_{L2} = 20.61\,[\Omega]. \tag{20}$$

From (17) and (19), the reactance x_F in the F section is

$$x_F = x_G - x_{FG} = -235.2\,[\Omega]. \tag{21}$$

Parallel resistance R_E is expressed by the load resistance R_{DE} and the parallel resistance R_D in Fig. 8(d), i.e.,

$$\frac{1}{R_E} = \frac{1}{R_{DE}} + \frac{1}{R_D} \tag{22}$$

where the resistance R_{DE} is equal to the load resistance R. Power P_E consumed in section E is expressed as

$$P_E = P_O + P_D = P_O + P_{AB} + P_A \tag{23}$$

where the power P_A includes the power losses $P_{\rm div}$ in the dividing resistors and the power loss P_g in the gate resistance of the MOSFET. The power P_E could be also expressed by

$$P_E = \frac{V_E^2}{R_E} \tag{24}$$

where V_E is the rms value of the output sinusoidal voltage v_O. The power P_D is similarly obtained

$$P_D = P_{AB} + P_A = \frac{V_E^2}{R_D}. \tag{25}$$

Parallel resistance R_A is composed of parallel gate–source resistance $R_{\rm gs}$, upper dividing resistance R_{d1}, and bottom dividing resistance R_{d2}

$$\frac{1}{R_A} = \frac{1}{R_{\rm gs}} + \frac{1}{R_{d1}} + \frac{1}{R_{d2}}. \tag{26}$$

Assuming that IRFR120Z [26] is selected as switch S, its threshold voltage $V_{\rm th}$ is 3 [V]. Since the input voltage $V_{\rm IN} = 6$ [V] is given, the upper dividing resistance R_{d1} and the bottom dividing resistance R_{d2} are equally 650.0 [kΩ]. Measured gate input impedance $z_{\rm gs}$ of IRFR120Z is

$$z_{\rm gs} = r_{\rm gs} + jx_{\rm gs} = r_{\rm gs} - j\frac{1}{\omega C_{\rm gs}} = 12.20 - j434.4\,[\Omega]. \tag{27}$$

Therefore, reactance factor $q_{\rm gs}$ of the gate–source is

$$q_{\rm gs} = \frac{x_{\rm gs}}{r_{\rm gs}} = -35.61. \tag{28}$$

From (8), (27), and (28), parallel resistance $R_{\rm gs}$ is obtained as

$$R_{\rm gs} = r_{\rm gs}(1 + q_{\rm gs}^2) = 15.48\,[\text{k}\Omega]. \tag{29}$$

From (28) and (29), the parallel reactance $X_{\rm gs}$ is obtained as

$$X_{\rm gs} = \frac{R_{\rm gs}}{q_{\rm gs}} = -434.7\,[\Omega]. \tag{30}$$

From (26), (29), and the dividing resistances R_{d1} and R_{d2}, parallel resistance R_A is determined as $R_A = 14.78$ [kΩ]. When no reactance component exists expect the switch in the A section, i.e., $X_A = X_{\rm gs}$, from (30), the reactance factor q_A is

$$q_A = \frac{R_A}{X_A} = \frac{R_A}{X_{\rm gs}} = -34.00. \tag{31}$$

From (9) and (31), the resistance r_A is

$$r_A = \frac{R_A}{(1 + q_A^2)} = 12.77\,[\Omega]. \tag{32}$$

From (7), (31), and (32), the reactance x_A is

$$x_A = q_A r_A = -434.2\,[\Omega]. \tag{33}$$

The maximum gate-to-source voltage $V_{\rm gsm}$ is determined to 10 [V], which is within the range of gate–source voltage of IRFR120Z [26]. The maximum current $I_{\rm Am}$ through the A section is

$$I_{\rm Am} = \frac{V_{\rm gsm}}{|Z_A|} = \frac{V_{\rm gsm}}{\sqrt{r_A^2 + x_A^2}} = 23.02\,[\text{mA}]. \tag{34}$$

Power loss caused by the ESR of the inductor L_4 is taken into account for the design. From the initial condition 5), (25), (32), and (34), the power P_D is estimated as

$$P_D = P_{AB} + P_A = \frac{1}{2}I_{\rm Am}^2 r_{AB} + \frac{1}{2}I_{\rm Am}^2 r_A = 3.649\,[\text{mW}]. \tag{35}$$

From (23) and (25), the ratio k_p of the power P_E to the power P_D is defined by

$$k_p = \frac{P_E}{P_D} = \frac{P_O + P_D}{P_D} = 275.0 \tag{36}$$

where k_p is also expressed by $k_p = R_D/R_E$. Moreover, from (22) and (36), the parallel resistances R_E and R_D are

$$R_E = R_{DE}\left(1 - \frac{1}{k_p}\right) = 49.82\,[\Omega] \tag{37}$$

$$R_D = R_{DE}\,(k_p - 1) = 13.70\,[\text{k}\Omega]. \tag{38}$$

From (10), (20), and (37), the reactance factor q_E is

$$q_E = -\sqrt{\frac{R_E}{r_E} - 1} = -1.190. \tag{39}$$

From (16) and (39), the phase difference φ_{EG} is

$$\varphi_{EG} = \arctan q_E - \arctan q_G = -1.637\,[\text{rad}]. \tag{40}$$

From (37) and (39), the parallel reactance X_E is

$$X_E = \frac{R_E}{q_E} = -41.87\,[\Omega]. \tag{41}$$

From (20) and (39), the reactance x_E is

$$x_E = q_E r_E = -24.53\,[\Omega]. \tag{42}$$

From (21) and (42), the reactance x_{EF} is

$$x_{EF} = x_F - x_E = -210.7\,[\Omega]. \tag{43}$$

Because no reactance component exists in the D–E section, $X_D = X_E$. From (38) and (41), we obtain

$$q_D = \frac{R_D}{X_D} = \frac{R_D}{X_E} = -327.2. \tag{44}$$

From (9), (38), and (44), the resistance r_D is

$$r_D = \frac{R_D}{1 + q_D^2} = 0.1280\,[\Omega]. \tag{45}$$

From (44) and (45), the reactance x_D is

$$x_D = q_D r_D = -44.88\,[\Omega]. \tag{46}$$

The phase shift of the fundamental component from drain to gate of the MOSFET should be zero or $2\pi n$ [rad] (n is an integer

number). From (4), the phase difference φ_{AG} is set to

$$\begin{aligned}\varphi_{AG} &= \varphi_{EG} + \varphi_{CD} + \varphi_{AB} \\ &= \varphi_{EG} + (\arctan q_C - \arctan q_D) \\ &\quad + (\arctan q_A - \arctan q_B) = -3.297\,[\text{rad}]. \end{aligned} \tag{47}$$

Here, the reactance factor q_D = –327.2 and q_A = 34.00 are already derived. However, the reactance factor q_C, and q_B are unknown. Assuming that difference θ between impedance arguments is

$$\theta = \arctan q_C - \arctan q_B \tag{48}$$

from (31), (40), (44), and (47) the phase difference θ is determined to

$$\begin{aligned}\theta = &\arctan q_C - \arctan q_B = \varphi_{AG} - \varphi_{EG} \\ &- \arctan q_A + \arctan q_D = -1.686\,[\text{rad}]. \end{aligned} \tag{49}$$

When no resistance component exists in the B–C section, $R_C = R_B$, i.e.,

$$r_B\left(1 + q_B^2\right) = r_C\left(1 + q_C^2\right). \tag{50}$$

From (32) and Condition 5) the ESR r_{AB} of the inductor L_4 = 1.000 [Ω], the series resistance r_B is

$$r_B = r_A + r_{AB} = 13.77\,[\Omega]. \tag{51}$$

When no resistance component exists in the C–D section, i.e., $r_C = r_D$, from (50), the reactance factor q_B is

$$q_B = \pm\sqrt{\frac{r_D}{r_B}\left(1 + q_C^2\right) - 1}. \tag{52}$$

From (45), (49), (51), and [23, eq. (A16)], the reactance factor q_C is

$$q_C = \begin{cases} \dfrac{1}{\tan\theta}\left[\sqrt{\dfrac{r_B}{r_D}\left(1 + \tan^2\theta\right)} - 1\right] = 10.36 \\ \dfrac{1}{\tan\theta}\left[-\sqrt{\dfrac{r_B}{r_D}\left(1 + \tan^2\theta\right)} - 1\right] = -10.56. \end{cases} \tag{53}$$

From (45), (51), and (53), the reactance factor q_B is

$$q_B = \begin{cases} \pm\sqrt{\dfrac{r_D}{r_B}\left(1 + q_C^2\right) - 1} = \pm 0.08358 \\ \pm\sqrt{\dfrac{r_D}{r_B}\left(1 + q_C^2\right) - 1} = \pm 0.2127. \end{cases} \tag{54}$$

From (53) and (54), the solutions applicable to (49) are

$$q_B = 0.2127 \tag{55}$$

$$q_C = -10.56. \tag{56}$$

From (51) and (55), reactance x_B is

$$x_B = q_B r_B = 2.929\,[\Omega]. \tag{57}$$

From (33) and (57), reactance x_{AB} is

$$x_{AB} = x_B - x_A = 437.1\,[\Omega]. \tag{58}$$

From (51) and (55), the parallel resistance R_B is

$$R_B = r_B\left(1 + q_B^2\right) = 14.39\,[\Omega]. \tag{59}$$

From (59) and (55), the parallel reactance X_B is

$$X_B = \frac{R_B}{q_B} = 67.65\,[\Omega]. \tag{60}$$

From (59) and (56), the parallel reactance X_C is

$$X_C = \frac{R_C}{q_C} = \frac{R_B}{q_C} = -1.363\,[\Omega]. \tag{61}$$

From (60) and (61), the parallel reactance X_{BC} is

$$X_{BC} = \frac{X_B X_C}{X_B - X_C} = -1.336\,[\Omega]. \tag{62}$$

From (45) and (56), the parallel reactance x_C is

$$x_C = q_C r_C = q_C r_D = -1.352\,[\Omega]. \tag{63}$$

From (46) and (63), the parallel reactance x_{CD} is

$$x_{CD} = x_D - x_C = -43.53\,[\Omega]. \tag{64}$$

Capacitances and inductances are determined by the above-mentioned equations. The output capacitance of IRFR120Z C_{ds} is 17 [pF] [26]. From (15), the capacitance C_1 is

$$C_1 = \left|\frac{1}{\omega X_{\text{HI}}}\right| - C_{\text{ds}} = 1.937\,[\text{nF}]. \tag{65}$$

From (43), the capacitance C_2 is

$$C_2 = \left|\frac{1}{\omega X_{EF}}\right| = 0.9440\,[\text{nF}]. \tag{66}$$

From (64), the capacitance C_{31} is

$$C_{31} = \left|\frac{1}{\omega x_{CD}}\right| = 4.570\,[\text{nF}]. \tag{67}$$

From (62), the capacitance C_{32} is

$$C_{32} = \left|\frac{1}{\omega X_{BC}}\right| = 148.9\,[\text{nF}]. \tag{68}$$

From (58), the inductance L_4 is

$$L_4 = \frac{x_{AB}}{\omega} = 86.96\,[\mu\text{H}]. \tag{69}$$

The resonant circuit L_3–C_3 has zero impedance at the third harmonic. Constraints of resonant circuit L_3–C_3 is

$$\omega^2 = \frac{1}{9L_3C_3}. \tag{70}$$

Determining the capacitance C_3 = 100.0 [pF], the inductance L_3 becomes 43.98 [μH].

IV. Simulation Results

To confirm the designed circuit operation under the ideal condition, the designed Class E/F$_3$ tuned power oscillator was simulated with LTspice 4.23 h. The switch parameter contains the threshold voltage V_{th} = 3.0 [V], the drain–source capacitance C_{ds} = 17.00 [pF], the gate–source resistance r_{gs} = 12.20 [Ω], and the gate–source capacitance C_{gs} = 0.4580 [nF]. The simulation waveforms are shown in Fig. 9. In Fig. 9(a), the input current was almost constant, which was nearly 176.3 [mA]. In Fig. 9(b), the switch voltage waveform v_{DS} achieved ZVS and ZVDS at

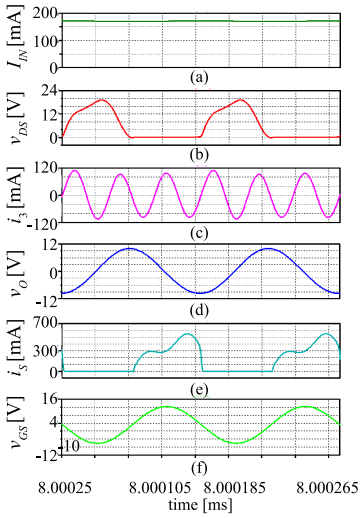

Fig. 9. Simulation waveforms, (a) the input voltage $V_{\rm IN}$, (b) the third harmonic component current i_3, (c) the switch current i_S, (d) the drain–source voltage $v_{\rm DS}$, (e) the output voltage v_O, and (f) the gate–source voltage $v_{\rm GS}$.

turning ON. And the switch voltage stress $V_{\rm DS}$ was 19.05 V, which was about the same to the theoretical switch voltage stress $V_{\rm DS}$ = 18.90 [V]. In Fig. 9(c), the third harmonic component current i_3 was in sinusoidal waveform, which had three times the frequency of the operation frequency. The amplitude I_3 of the third harmonic component current was ideally 78.60 [mA]; however, in the simulation I_3 was nearly 115.0 [mA]. The difference in the amplitude of the third harmonic component current is due to the difference between the theoretical value and the designed value. The output voltage v_O was in sinusoidal waveform under the load quality factor $Q = 12$ as shown in Fig. 9(d). In Fig. 9(e), the switch current i_S almost achieved ZCS at turning ON. The gate–source voltage $v_{\rm GS}$ was also in sinusoidal waveform centered on the threshold voltage $V_{\rm th}$ as shown in Fig. 9(f). From Fig. 9(d) and (f), it can be seen that the phase difference between the output voltage and the gate–source voltage was –1.738 [rad], which was about the same as that of the theoretical phase difference $\varphi_{AE} = \varphi_{AG} - \varphi_{EG}$ = –1.660 [rad]. The simulation waveforms and the ideal waveforms were in good agreement. The power conversion efficiency was 94.61 [%] and the operation frequency was 800.0 [kHz].

V. Experimental Results

To confirm the circuit operation, a Class E/F$_3$ tuned power oscillator was built and tested. Experimental parameters are shown in Table II. Experimental waveforms of the input voltage $V_{\rm IN}$, the output voltage v_O, the drain–source voltage $v_{\rm DS}$, and the switch current i_S are shown in Fig. 10. The theoretical values, the simulation, and the experimental results are compared in Table III. In Fig. 10, the input voltage $V_{\rm IN}$ was almost constant. The output voltage v_O was in sinusoidal waveform, whose RMS value $V_{\rm ORMS}$ was 6.693 [V] and the frequency was 801.6 [kHz]. The power conversion efficiency was 86.24 [%]. The RMS value of the output voltage $V_{\rm ORMS}$ and the power conversion efficiency were lower than the theoretical value due to the ESRs of the

TABLE II
Experimental Parameters

	Theory (ESR [Ω])	Measured (ESR [Ω])	Difference [%]
R_{d1} [kΩ]	650.0	674.0	+3.692
R_{d2} [kΩ]	650.0	686.3	+5.585
RFC [mH]	2.200	2.247 (0.5921)	+2.136
C_1 [nF]	1.937	1.816 (0.3089)	−6.247
L_2 [μ H]	50.87	49.81 (0.6977)	−2.084
C_2 [nF]	0.9440	0.9165 (1.354)	−2.913
L_3 [μ H]	43.98	45.65 (1.002)	−3.797
C_3 [pF]	100.0	97.31 (0.5267)	−2.690
R [Ω]	50.00	49.36	−1.270
C_{31} [nF]	4.570	4.513 (0.1220)	−01.247
C_{32} [nF]	148.9	148.3 (0.3497)	−0.4030
L_4 [μ H]	86.96 (1.000)	85.37 (1.046)	−1.828 (+4.600)

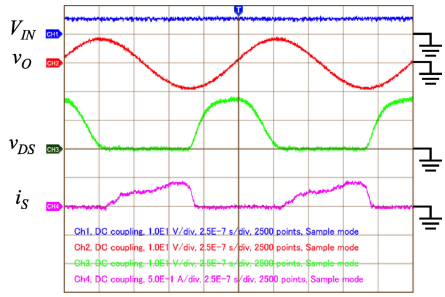

Fig. 10. Experimental waveforms of the input voltage $V_{\rm IN}$, the output voltage v_O, the drain–source voltage $v_{\rm DS}$, and the switch current i_S, $V_{\rm IN}$: 10 V/div, v_O: 10 V/div, i_S: 500 mA/div, horizontal: 250 ns/div.

TABLE III
Calculated Value of the Oscillator, Simulation and Experimental Results

	Theory	Simulation	Measured
$V_{\rm DS}$ [V]	18.90	19.05	18.20
I_S [mA]	565.9	541.9	450.0
f [kHz]	800.0	800.0	801.6
$V_{\rm IN}$ [V]	6.000	6.000	6.003
$I_{\rm IN}$ [A]	0.1851	0.1763	0.1753
$P_{\rm IN}$ [W]	1.111	1.058	1.052
$V_{\rm ORMS}$ [V]	7.071	7.075	6.693
P_O [W]	1.000	1.001	0.9075
η [%]	90.00	94.61	86.24
φ_{AE} [rad]	–1.660	–1.738	–1.772

passive elements and the switch ON resistance $r_{\rm ON}$. The switch current i_S almost achieved ZCS at turning ON, and the switch voltage waveform $v_{\rm DS}$ achieved ZVS and ZVDS at turning ON. The theoretical, simulation, and experimental waveforms of the switch current and the switch voltage were in good agreement. The switch voltage stress $V_{\rm DS}$ was 18.20 [V], and it was close to the theoretical and simulation values. The switch current stress I_S was 450.0 [mA], which was lower than the theoretical and the simulation values. It could be caused by the decreasing of the output current i_O. Experimental waveforms of the input current $I_{\rm IN}$, the shunt capacitance current i_{C1}, and the third harmonic component current i_3 are shown in Fig. 11. The averaged amplitude I_3 of the third harmonic component current was nearly 76.21 [mA]. Ringing in the capacitor current waveform

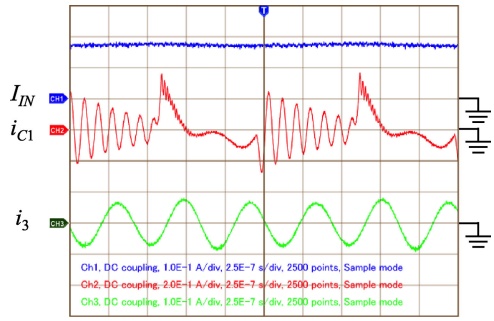

Fig. 11. Experimental waveforms of the input current $I_{\rm IN}$, the shunt capacitance current i_C, and the third harmonic component current i_3, $I_{\rm IN}$: 100 mA/div, i_C: 200 mA/div, i_3: 100 mA/div, horizontal: 250 ns/div.

i_{C1} could be caused by the resonance of the equivalent series inductance of the line and the drain–source capacitance $C_{\rm ds}$ of switch S.

VI. Conclusion

The Class E/F$_3$ tuned power oscillator has been proposed. Class E/F$_3$ oscillator satisfies ZVS and ZVDS at the turning ON instant, which decreases the switching loss. Moreover, the voltage stress of the switch is lower than Class E tuned power oscillator. The circuit operation has been verified by simulation and circuit experiment. The experimental results show good agreements with the theory and the simulation results. In the circuit experiments of the proposed oscillator, the measured oscillation frequency was 801.6 kHz, the output power was 0.9075 W, and the power conversion efficiency was 86.24 %.

References

[1] A. Grebennikov and N. O. Sokal, *Switchmode RF Power Amplifiers*, New York, NY, USA: Newnes, 2007.
[2] M. K. Kazimierczuk and D. Czarkowski, *Resonant Power Converter*, 2nd ed., Hoboken, NJ, USA: Wiley, 2011.
[3] N. Sokal and A. Sokal, "Class E—A new class of high-efficiency tuned single-ended switching power amplifiers," *IEEE J. Solid-State Circuits*, vol. SC-10, no. 3, pp. 168–176, Jun. 1975.
[4] F. H. Raab, "Idealized operation of class-E tuned power-amplifier," *IEEE Trans. Circuits Syst.*, vol. CS-24, no. 12, pp. 725–735, Dec. 1977.
[5] F. H. Raab, "Effects of circuit variations on the class E tuned power amplifier," *IEEE J. Solid-State Circuits*, vol. SC-13, no. 2, pp. 239–247, Apr. 1978.
[6] F. H. Raab and N. O. Sokal, "Transistor power losses in the class E tuned power amplifier," *IEEE J. Solid-State Circuits*, vol. SC-13, no. 6, pp. 912–914, Dec. 1978.
[7] N. O. Sokal and A. D. Sokal, "High efficiency tuned switching power amplifier," U.S. Patent 3 919 656, Nov. 11, 1975.
[8] J. Ebert and M. Kazimierczuk, "High efficiency RF power amplifier," *Bull. Acad. Pol. Sei., Sen Sei. Tech.*, vol. 25, no. 2, pp. 13–16, Feb. 1977.
[9] D. J. Kessler and M. K. Kazimierczuk, "Power losses and efficiency of class-E power amplifier at any duty ratio," *IEEE Trans. Circuits Syst. I, Reg. Papers*, vol. 51. no. 9, pp. 1675–1689, Sep. 2004.
[10] J. Cumana, A. Grebennikov, G. Sun, N. Kumar, and R. H. Jansen, "An extended topology of parallel-circuit class-E power amplifier to account for larger output capacitances," *IEEE Trans. Microw. Theory Tech.*, vol. 59, no. 12, pp. 3174–3183, Dec. 2011.
[11] F. H. Raab, "Class-F power amplifiers with maximally flat waveforms," *IEEE Trans. Microw. Theory Tech.*, vol. 45, no. 11, pp. 2007–2012, Nov. 1997.
[12] F. H. Raab, "Maximum efficiency and output of class-F power amplifiers," *IEEE Trans. Microw. Theory Tech.*, vol. 49, no. 6, pp. 1162–1166, Jun. 2001.
[13] F. H. Raab, "Class-E, class-C, and class-F power amplifiers based upon a finite number of harmonics," *IEEE Trans. Microw. Theory Tech.*, vol. 49, no. 8, pp. 1462–1468, Aug. 2001.
[14] S. Kee, "The class E/F family of harmonic-tuned switching power amplifiers," Ph.D. dissertation, California Inst. Technol., Pasadena, CA, USA, 2001.
[15] S. D. Kee, I. Aoki, A. Hajimiri, and D. Rutledge, "The class E/F family of ZVS switching amplifiers," *IEEE Trans. Microw. Theory Tech.*, vol. 51, no. 6, pp. 1677–1690, Jun. 2003.
[16] Z. Kaczmarczyk, "High-efficiency class-E, EF$_2$ and E/F$_3$ inverters," *IEEE Trans. Ind. Electron.*, vol. 53, no. 5, pp. 1584–1593, Oct. 2006.
[17] A. Grebennikov, "High-efficiency class-FE tuned power amplifiers," *IEEE Trans. Circuits Syst. I, Reg. Papers*, vol. 55, no. 11, pp. 3284–3292, Nov. 2008.
[18] F. You, S. He, X. Tang, and X. Deng, "High-efficiency single-ended classe/F$_2$ power amplifier with finite dc feed inductor," *IEEE Trans. Microw. Theory Tech.*, vol. 58, no. 1, pp. 32–40, Jan. 2010.
[19] S. Aldhaher, "Modeling and analysis of class EF and class E/F inverters with series-tuned resonant networks," *IEEE Trans. Power Electron.*, vol. 30, no. 5, pp. 3415–3430, May 2016.
[20] A. Grebennikov, "High-efficiency class E/F lumped and transmissionline power amplifiers," *IEEE Microw. Theory Trans.*, vol. 59, no. 6, pp. 1579–1588, Jun. 2011.
[21] J. Ebert and M. K. Kazimierczuk, "Class E high-efficiency tuned power oscillator," *IEEE J. Solid-State Circuits*, vol. SC-16, no. 2, pp. 62–66, Apr. 1981.
[22] M. K. Kazimierczuk, "A new approach to the design of tuned power oscillators," *IEEE Trans. Circuits Syst.*, vol. CAS-29, no. 4, pp. 261–267, Apr. 1982.
[23] M. K. Kazimierczuk, V. G. Krizhanovski, J. V. Rassokhina, and D. V. Chernov, "Class-E plbibsc-mosfet tuned power oscillator design procedure," *IEEE Trans. Circuits Syst. I, Reg. Papers*, vol. 52, no. 6, pp. 1138–1147, Jun. 2005.
[24] H. Hase, H. Sekiya, J. Lu, and T. Yahagi, "Resonant dc/dc converter with class E oscillator," *IEEE Trans. Circuits Syst. I, Reg. Papers*, vol. 53, no. 9, pp. 2025–2035, Sep. 2006.
[25] D. V. Chernov, M. K. Kazimierczuk, and V. G. Krizhanovski, "Class-E plbibsc-mosfet low-voltage power oscillator," in *Proc. IEEE Int. Symp. Circuits Syst.*, Phoenix, AZ, USA, vol. 5, May 2002, pp. 509–512.
[26] *IRFR120Z date-sheet*. 2003. [Online]. Available: http://www.irf.com/product-info/datasheets/data/irfr120z.pdf

Tsuyoshi Inaba (S'16) received the B.E. degree in electrical engineering from Tokyo University of Science, Tokyo, Japan, in 2016. He is currently working toward the M.E. degree in electrical engineering at Tokyo University of Science.

His research interests include high-frequency inverter and resonant dc/dc power converters.

Hirotaka Koizumi (S'98–M'01) was born in Tokyo, Japan, in 1970. He received the B.E., M.E., and Ph.D. degrees in electrical engineering from Keio University, Yokohama, Japan, in 1993, 1995, and 2001, respectively.

From 1995 to 2001, he was an Electrical Engineer in Tokyo Electric Power Company Inc., Tokyo, Japan. From 1998 to 2001, he was in the Graduate School, Keio University. From 2001 to 2007, he was at Tokyo University of Agriculture and Technology, Tokyo, Japan, as a Research Associate. Since April 2007, he has been at Tokyo University of Science, Tokyo, Japan, where he is currently a Professor. His research interests include photovoltaic systems, high-frequency high-efficiency tuned power amplifiers, resonant dc/dc power converters, dc/ac inverters, and high-frequency rectifiers.

Dr. Koizumi is a member of the Institute of Electrical Engineers of Japan, and the Institute of Electronics, Information, and Communication Engineers of Japan. From May 2008 to May 2010, he was the Secretary of the IEEE Circuits and Systems Society Power Systems and Power Electronic Circuits Technical Committee. From May 2012 to May 2013 and from May 2013 to May 2014, he was the Chair and the Past Chair of the IEEE Circuits and Systems Society Power and Energy Circuits and Systems Technical Committee.